

Establishing an Animal Model of Cytomegalovirus Keratouveitis in Rats: Broad Infection of Anterior Segment Tissue by Cytomegalovirus

Shuang Zhang,¹ Yunxiao Zang,¹ Qing Lu,¹ Jiao Ma,¹ Xuan Jiang,² Jinghao Qu,¹ Jiixin Zhang,¹ Rongmei Peng,¹ Minhua Luo,² and Jing Hong¹

¹Department of Ophthalmology, Peking University Third Hospital, Beijing Key Laboratory of Restoration of Damaged Ocular Nerve, Peking University Third Hospital, Haidian District, Beijing, China

²State Key Laboratory of Virology, CAS Center for Excellence in Brain Science and Intelligence Technology, Center for Biosafety Mega-Science, Wuhan Institute of Virology, Chinese Academy of Sciences, Wuhan, China

Correspondence: Jing Hong, Department of Ophthalmology, Peking University Third Hospital, Beijing Key Laboratory of Restoration of Damaged Ocular Nerve, Peking University Third Hospital, No. 49 North Garden Road, Haidian District, Beijing 100191, China; hongjing196401@163.com.

First author: Shuang Zhang; zshuang95@qq.com.

Received: May 15, 2021

Accepted: September 27, 2021

Published: October 26, 2021

Citation: Zhang S, Zang Y, Lu Q, et al. Establishing an animal model of cytomegalovirus keratouveitis in rats: Broad infection of anterior segment tissue by cytomegalovirus. *Invest Ophthalmol Vis Sci.* 2021;62(13):22. <https://doi.org/10.1167/iovs.62.13.22>

PURPOSE. Considering the difficulty of obtaining adequate biological tissue in clinical practice, we established an animal model of cytomegalovirus (CMV) keratouveitis in rats and investigated the viral infection sites and corresponding imaging and histopathological features.

METHODS. Subconjunctival injection and topical use of dexamethasone were used to induce ocular immunosuppression in rats followed by intracameral inoculation of murine cytomegalovirus (MCMV). The clinical manifestations, intraocular pressure (IOP) and imaging changes were observed. Infected eyes were further examined by immunofluorescence, light microscopy, and electron microscopy. MCMV RNA was detected by reverse transcription-polymerase chain reaction.

RESULTS. Typical keratouveitis occurred in the experimental rats and was characterized by corneal edema, keratic precipitates, and iridocyclitis with increased IOP. Corneal endothelial lesions displayed as “black holes,” enlarged intercellular gaps, and high-intensity cellular infiltration by confocal microscopy, consistent with the pathological changes of “ballooning degeneration,” endothelial cell detachment, and inflammatory cell infiltration. Mitochondrial edema was the most prominent organelle lesion in endothelial cells. Trabeculitis, mechanical obstruction of Schlemm’s canal, and anterior chamber angle stenosis accounted for elevated IOP. Inflammation of the iris and ciliary body tended to transform into a chronic form. Immunofluorescence revealed that corneal endothelial cells, iris cells, trabecular meshwork cells, and monocytes could be infected by MCMV. MCMV RNA was found in the anterior segments after infection.

CONCLUSIONS. CMV can widely infect anterior segment tissue, including the corneal endothelium, iris, and trabecular meshwork, in vivo, inducing the corresponding clinical manifestations. Corneal endotheliitis and hypertensive anterior uveitis could be the specific stage of anterior segment infection of CMV.

Keywords: cytomegalovirus, keratouveitis, animal model, pathological change

With the wide application of the polymerase chain reaction (PCR) in clinical practice, many ocular anterior segment diseases previously with unknown etiologies have been found to be closely associated with viral infections.^{1–4} In Asia-Pacific regions, cytomegalovirus (CMV) is the most common cause of corneal endotheliitis,^{5–8} characterized by localized corneal edema, coin-shaped keratic precipitates (KPs), and mild anterior chamber reactions.⁹ Although the diagnosis of typical CMV corneal endotheliitis is not difficult, the condition can be complicated with diffuse corneal edema, making the shapes of KPs hard to confirm. In addition, accumulating evidence has demonstrated that CMV might be an important etiological factor for hypertensive anterior uveitis (HAU) in immunocompetent patients.^{3,10–13} According to recent studies, the prevalence of CMV in the

aqueous humor associated with HAU varies from 19% to 28.5%,^{11,13,14} and patients with CMV positivity respond well to antiviral treatment. CMV anterior uveitis usually presents as recurrent episodic iritis with raised intraocular pressure (IOP) resembling Posner-Schlossman syndrome (PSS) or as a chronic form mimicking Fuch’s heterochromatic iridocyclitis.¹³ Between 60 and 93.3%^{13,15–17} of CMV-related HAU has been reported to manifest as PSS, and Chee et al.² revealed that CMV was found in 52.2% of patients with PSS.

In fact, there seem to be no definite boundaries among CMV corneal endotheliitis, CMV anterior uveitis, and PSS. Patients usually have overlapping features of these diseases simultaneously, or certain diseases seem to occur successively in patients during the whole course. Koizumi et al.⁹ discovered that patients with CMV endotheliitis

commonly had a history of recurrent anterior uveitis and ocular hypertension. Similarly, Kam et al.¹⁸ reported that prior to PCR confirmation of CMV endotheliitis, 70.6% of patients were labeled as having anterior uveitis, and 41.2% were diagnosed with PSS. In turn, corneal endothelial loss was not rare in CMV anterior uveitis or PSS with high viral loads.¹⁹ All the above-mentioned findings suggest that corneal endotheliitis, anterior uveitis, or PSS might belong to the same spectrum of diseases and occur successively in the specific phase of CMV anterior segment infection.

Currently, the pathogenesis of CMV anterior segment infection is still not clear. Despite the abundance of clinical observations, basic research on this aspect is far from sufficient. In the real world, it is difficult to monitor the dynamic changes in clinical manifestations at different stages and obtain adequate biological tissue for pathological analysis. Therefore, establishing an effective animal model is necessary to further study the pathogenic mechanism of CMV infection. In a previous study, our team demonstrated that murine cytomegalovirus (MCMV) could infect rat corneal endothelial cells (RCECs) in vitro and in vivo.²⁰ Furthermore, we optimized the protocol to establish an animal model of CMV keratouveitis in rats and tried to confirm whether CMV could infect various anterior segment tissues of rats in vivo, resulting in clinical features similar to those we observe in clinical practice. In addition, we also investigated the relationships between clinical manifestations and corresponding imaging and histopathological changes at different stages after infection.

MATERIALS AND METHODS

Animals

Female Sprague-Dawley rats (180–200 g) at 6–8 weeks of age were used. The rats of different groups were housed in separate cages. We kept all the animals strictly in compliance with the ARVO Statement for the Use of Animals in Ophthalmic and Vision Research. The experimental protocol was approved by the Peking University Institutional Review Board Animal Welfare Committee (Approval No: LA2019348).

Virus

MCMV-enhanced-green fluorescent protein (eGFP; K181 strain) was obtained courtesy of Minhua Luo's research group, Wuhan Institute of Virology, Chinese Academy of Sciences. The MCMV genome was cloned and maintained as a 230 kb bacterial artificial chromosome (BAC) expressing eGFP under the control of the immediate early (IE) promoter. The viral titer was 2×10^4 plaque forming units (PFUs) per mL. MCMV was UV-inactivated by exposure to 100 mJ/cm² UV by using a UV cross-linker (CL-1000 Ultraviolet Crosslinker; UVP, LLC, Upland, CA, USA).

Infection of RCECs with MCMV-eGFP

To test MCMV tropism in RCECs, the RCECs were infected with MCMV in vitro. Primary cultured RCECs were obtained and propagated, as described previously.²⁰ Briefly, rat Descemet's membranes with RCECs were stripped off and digested with 1 mg/mL collagenase A at 37°C for 15 minutes. The RCECs were then suspended in culture medium and prepared in DMEM with 15% fetal bovine serum (FBS),

50 U/mL penicillin, and 50 g/mL streptomycin. Confluent cells were washed in Ca²⁺- and Mg²⁺-free Dulbecco's phosphate-buffered saline (PBS) and incubated with 0.25% trypsin-EDTA for 5 minutes at 37°C. Passage 2 RCECs were used for the experiment.

Confluent RCECs were seeded on coverslips in 48-well plates, and the cell numbers were counted. MCMV-eGFP suspended in cell culture medium was added at 100 pfu/5 μ l to each well, corresponding to a low multiplicity of infection (MOI) of 0.01. The same volume of DMEM (5 μ l) was added to the control group. The RCECs were then subjected to confocal microscopy examination (Leica TCS SP8, Wetzlar, Germany) at 1–10 days postinfection (dpi).

Experimental Design of the CMV Keratouveitis Model

Part one: Twenty-four rats were randomly divided into three groups. The rats were anesthetized by intraperitoneal administration of 1% pentobarbital sodium (0.8 mL) beforehand in each invasive operation. The ocular suppression state was first induced by drug treatment in all the rats. The right eyes of all the rats received subconjunctival injection of dexamethasone (0.2 mL: 1 mg) from 3 o'clock on days 1, 4, and 7 and topical use of tobramycin and dexamethasone eye drops (Tobradex, Alcon-Couvreur) 4 times a day for 1 week. One week later, the MCMV group received right-eye intracameral inoculation of MCMV; anterior chamber paracentesis was performed through the rat corneal limbus at 3 o'clock by using a 5 μ l glass microsyringe (Series 600, Hamilton Company). We first extracted 3 μ l aqueous humor and then injected the same volume of viral suspension (60 PFU in 3 μ l) to eliminate its influence on the IOP. The UV-MCMV group received the same amount of UV-MCMV in the same manner; the UV-MOCK group received the same amount of UV-MOCK medium without virus. Clinical manifestations, IOP values, and imaging features were then monitored at 0, 1, 2, 3, 7, and 14 dpi consecutively.

Part two: One hundred forty-four rats were randomly separated into the MCMV-eGFP group, the UV-MCMV group, and the UV-MOCK group. The rats in the different groups were treated in the same manner described in part one. At different time points (0, 1, 2, 3, 7, and 14 dpi), eight rats in different groups were killed for histopathological examination. Two rats were sent for light microscopy examination, and two rats were sent for electron microscopy examination. Four rats were sent for immunofluorescence examination: two underwent corneal and iris dissection, and the other two were sent for frozen tissue sectioning.

Part three: Forty rats were separated into the MCMV-eGFP group and the UV-MCMV group and treated according to the methods in part one. At different time points (1, 2, 3, 7, and 14 dpi), four rats in each group were killed for reverse transcription-polymerase chain reaction (RT-PCR) examination. The RT-PCR examination was repeated three times for samples at each time point.

Slit-Lamp Examination

We investigated the clinical manifestations of the rats in the different groups at different time points by slit-lamp examination. We focused mainly on the degree of corneal edema, KPs, anterior chamber inflammation, and changes in the iris and pupil.

Protocol for IOP Examination

For each rat, IOP was measured with an iCare tonometer (Icare Finland) at different time points. One examiner held the rat rolled in a surgical drape and fixed each rat's head before anesthesia. The other examiner measured the eyes as close to the central cornea as possible without manual movement of its eyelids. Six values of the IOP were measured in rapid succession, and we repeated this process three times for each rat and calculated the final mean IOP. Twenty IOP values of the dexamethasone-treated experimental eyes and untreated contralateral eyes were obtained to confirm the normal range of rat IOP.

Imaging Examinations

All the rats underwent anterior segment optical coherence tomography (AS-OCT; Optovue, Fremont, CA, USA) and in vivo confocal microscopy (IVCM; Heidelberg Engineering, Heidelberg, Germany) after the slit-lamp examination. Corneal thickness changes, anterior chamber inflammation, and pupil changes were investigated with AS-OCT. In addition, the central corneal thickness (CCT) was monitored at different postinfection times with OCT. Finally, we scanned the rat corneas repeatedly for corneal endothelial lesions with IVCM.

Histological Examination With Light Microscopy

Intact rat eyes were collected and fixed in 4% paraformaldehyde at 4°C overnight. Whole rat eyes were placed in processing cassettes for routine dehydration through a serial alcohol gradient. Then, the tissues were embedded in paraffin wax blocks. Eye tissue sections (4-µm thick) were made (Leica RM2235, Germany) followed by dewaxing and rehydration. After that, hematoxylin and eosin (H&E) staining was performed, and sections were dehydrated again with ethanol and xylene. Viral cytopathic features and inflammatory changes in the anterior segment were analyzed.

Fluorescence Examination by Two-Photon Confocal Microscopy

In part two of the experiment, four eyeballs in different groups were obtained for viral fluorescence examination at different time points. Two of them were kept in 4% paraformaldehyde at 4°C overnight. After full fixation, corneal buttons and iris/ciliary bodies were completely dissected and separated in individual Eppendorf (EP) tubes. The tissues were washed 3 times in PBS and then incubated in TRITC rhodamine phalloidin (0.2 U/µl; YEASEN, Shanghai, China) for 10 minutes to label the F-actin of the cytoskeleton; next, the tissues were washed 3 more times in PBS and incubated in Hoechst 33258 (1 mg/mL; Solarbio, Beijing, China) for 10 minutes to label the cell nucleus. Finally, we spread the cornea buttons and iris/ciliary body carefully on glass slides and added antifade mounting medium (APPLYGEN, Beijing, China). Then, the tissues were covered with coverslips and sent for two-photon confocal microscopy examination (Leica TCS SP8, Wetzlar, Germany).

The other two eyeballs were processed with standard frozen tissue section procedures. They were placed in 2-mL EP tubes with OCT embedding agent (SAKURA, USA) and submerged in liquid nitrogen for 2 minutes. Subsequently, they were frozen in a -80°C refrigerator overnight. The next

day, 5-µm-thick frozen eye tissue sections were made (Leica CM1950, Germany). The frozen sections were incubated in the same manner as described above. The infection sites in the corneal endothelium, iris, and trabecular meshwork (TM) were detected afterward under two-photon microscopy.

Electron Microscopy Examination

For electron microscopy examination, corneas and irises/ciliary bodies were completely dissected and fixed in 2.5% glutaraldehyde at 4°C overnight. Then, all the samples were washed in PBS 3 times and fixed in 1% osmic acid at 4°C for 2 hours. After that, the samples were dehydrated through a series of acetone gradients (30%, 50%, 70%, 90%, and 100%). We submerged all the samples in a 1:1 mixture of 100% acetone and embedding agent for 1 hour and then transferred them to the embedding capsule with embedding agent. The samples were incubated in a 37°C thermostat overnight, followed by incubation at 60°C for 48 hours; 50-nm sections were made and stained with acetic acid glaze and lead citrate. We observed all the sections under transmission electron microscopy (TEM; Hitachi SU8010, Japan).

Detection of MCMV RNA by RT-PCR Examination

All the eyeballs were divided into two parts: anterior segment samples included the dissected corneas, irises, and ciliary bodies, and the posterior segment samples mainly contained retinas. At each time point, samples from four independent rats in the MCMV-eGFP group and UV-MCMV group were pooled for RNA extraction because the individual samples had a relatively low mass.

TRIzol reagent (Life Invitrogen, USA) was used to extract total RNA from ocular tissue samples according to the manufacturer's instructions. RNA samples were then reverse transcribed to produce cDNA templates in the presence of HiScript II Q RT SuperMix for qPCR (+gDNA wiper; R223-01; Vazyme Biotech, Nanjing, China). The reaction mixtures were then used for PCR.

Each PCR contained 1.0 µl of extracted cDNA (diluted 5 times), 2.0 µl of primers specific for the MCMV IE gene based on a previous publication²¹ (5'-GGCCGTCACCTTGGATGAGAAC-3'; 5'-TTACAGGACAACAGAACGCTC-3'; 258-bp product) and the rat β-actin gene (5'-GCCATGTACGTAGCCATCCA-3'; 5'-GAACCGCTCATTGCCGATAG-3'; 375-bp product), 12.5 µl 2 × Es Taq MasterMix (Dye; CW0690M; CWBIO, Beijing, China), and 9.5 µl RNase-free ddH₂O in a 25-µl final volume. Each cycle reaction included initial denaturation at 94°C for 3 minutes, denaturation at 94°C for 15 seconds, annealing at 55°C for 15 seconds, extension at 72°C for 15 seconds, and a final 5-minute extension period at 72°C. The samples underwent 30 cycles of amplification. The amplified DNA samples were electrophoresed on 2.5% agarose gels and scanned with ChemiDoc TM XRS+ (Bio-Rad, USA).

Statistical Analysis

We used the Statistical Package for the Social Sciences software, version 22.0 (SPSS Inc., Chicago, IL, USA) for statistical analysis. Comparisons of CCT and IOP values were performed with *t*-tests (the MCMV-eGFP group versus the UV-MCMV group or the UV-MOCK group). Categorical variables were analyzed by Fisher's exact test. A

P value < 0.05 was considered to indicate statistically significant differences.

RESULTS

MCMV Could Infect RCECs Effectively In Vitro

Although the RCECs were infected with MCMV-eGFP at a low MOI, green fluorescence-positive RCECs were detected as early as 2 dpi. As [Figure 1](#) shows, focal clusters of green-fluorescent RCECs were remarkable from 3 dpi. With the spread of infection, the extent of cell necrosis and quantity of eGFP-positive RCECs increased subsequently from 3 to 6 dpi. Few eGFP-positive RCECs were visible at 8 dpi and none at 10 dpi.

Typical Keratouveitis Occurred in the Rats After CMV Infection

The clinical manifestations of different rat groups are shown in [Figure 2](#), and the incidences of various clinical signs are displayed in [Table 1](#). All the rat eyes in the UV-MCMV and UV-MOCK groups retained the normal anterior segment appearance without obvious inflammatory changes, as shown in [Figure 2A](#). The corneas were transparent with the CCT fluctuating within the normal range based on AS-OCT (see [Fig. 2A g-j](#)). There were no inflam-

matory exudates, flares, or cells in the anterior chamber, and the iris texture was clear. In contrast, all the rats infected with MCMV-eGFP developed obvious keratouveitis, which was characteristic of concomitant corneal endotheliitis and anterior uveitis. Keratouveitis was aggravated in the initial 3 to 7 days after infection and was gradually alleviated within 2 weeks.

[Figure 2B](#) shows the features of corneal endotheliitis in the rats. After intracameral inoculation of MCMV, 62.5% of the rats developed localized corneal edema during the clinical course, which was detected with slit-lamp examination (see [Fig. 2B a,b](#)) and AS-OCT (see [Fig. 2B g](#)). Half of the rats exhibited diffuse corneal edema with severe ciliary injection (see [Fig. 2B c,d](#)). With the relief of corneal edema, sporadic large or medium mutton fat KPs were observed over the posterior surface of the cornea in 87.5% of the rats (see [Fig. 2B e,f](#)); these KPs were “hump”-like structures with high reflectivity on AS-OCT (see [Fig. 2B h,i](#)). [Figure 3](#) shows the CCT changes in different groups during the whole postinfection period. The CCT of the MCMV-eGFP group increased significantly in the initial 3 days (1–3 dpi) after infection ($P = 0.012$, < 0.001 , and < 0.001 compared with that of the UV-MCMV group; $P = 0.005$, < 0.001 , and < 0.001 compared with that of the UV-MOCK group). At 3 dpi, the CCT of the MCMV-eGFP group reached a peak value measuring $259.3 \pm 11.4 \mu\text{m}$ (mean \pm SEM), which was larger than those of the UV-MCMV group ($136.8 \pm 3.9 \mu\text{m}$) and the UV-MOCK

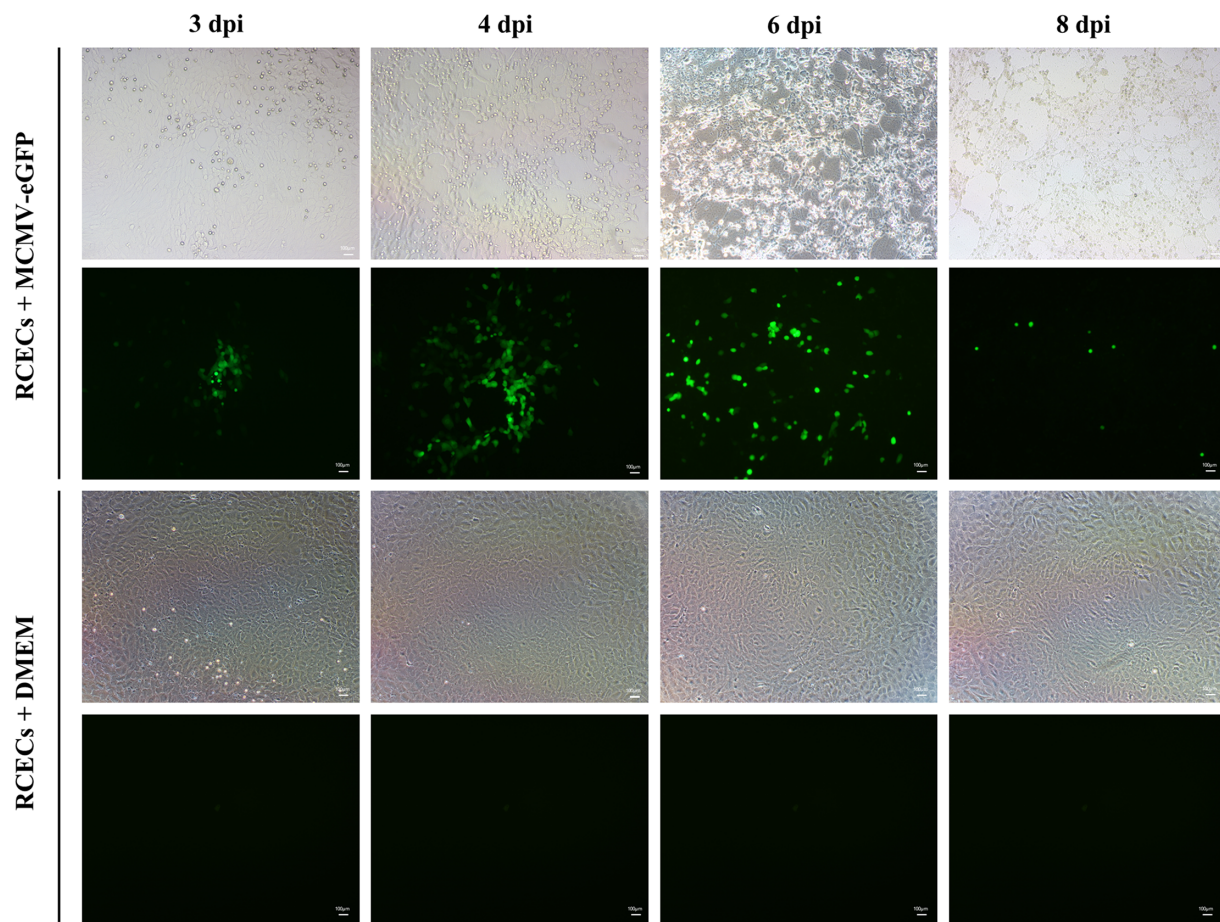


FIGURE 1. Infection of RCECs with MCMV in vitro. RCECs were inoculated with MCMV-eGFP at a low MOI. Green-fluorescent-positive RCECs in which MCMV was possibly replicated are shown at 3, 4, 6, and 8 dpi. dpi, days postinfection; bar = 100 μm .

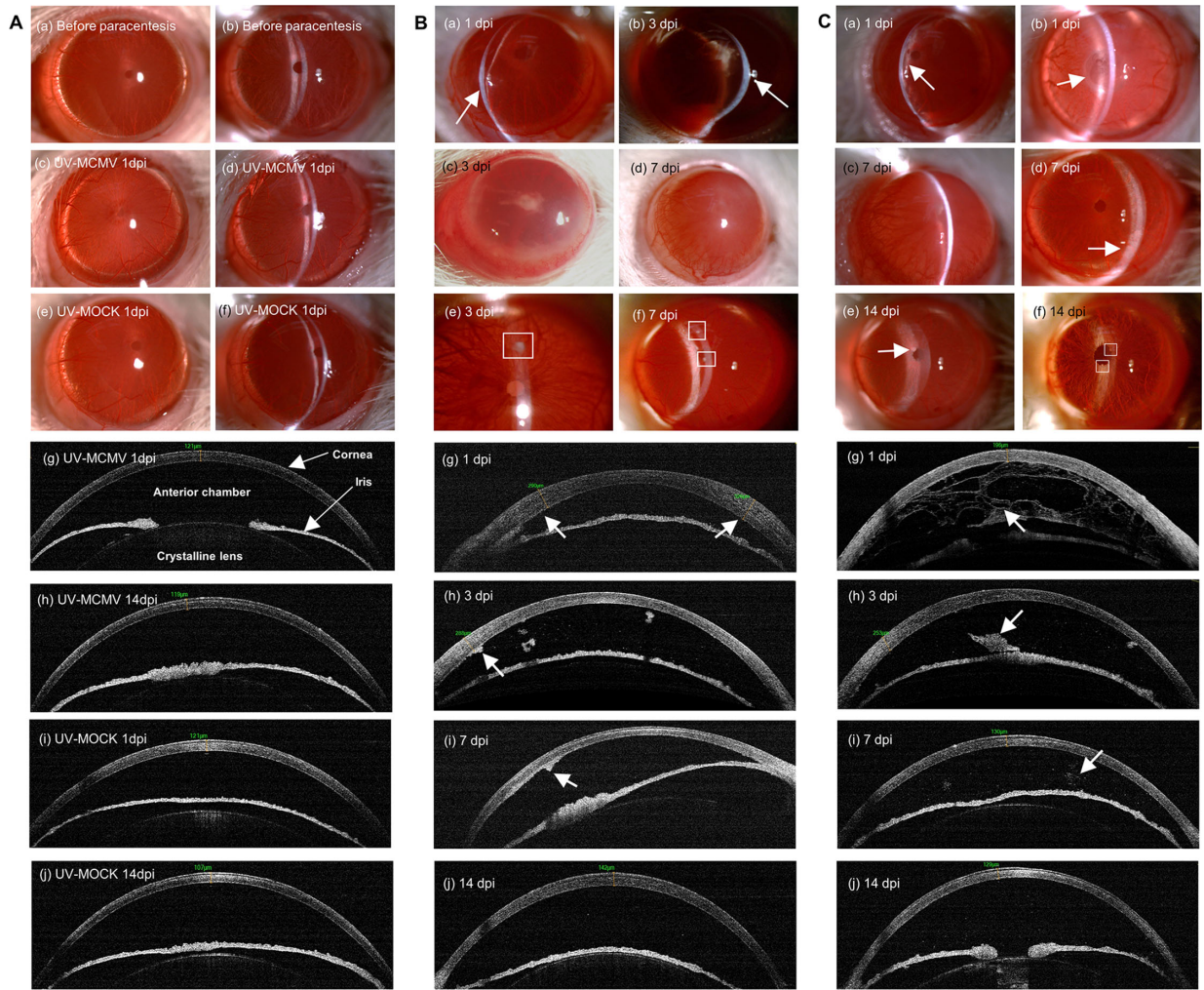


FIGURE 2. Clinical manifestations of CMV keratouveitis in rats by slit-lamp examination and AS-OCT. (A) Slit-lamp views and AS-OCT images of the anterior segment of the eyes in different control groups. (B) Representative images of corneal lesions in the MCMV group: (a, b) Localized corneal edema (white arrows); (c, d) Diffuse corneal edema; (e, f) Mutton fat KPs (white squares); (g) OCT view of uneven corneal edema (white arrows); (h, i) KPs exhibiting “hump”-like structures with high reflectivity by OCT (white arrow); (j) Corneal edema and anterior chamber inflammation relieved at 14 dpi. (C) Representative images of anterior uveitis in the MCMV group: (a) Diffuse anterior chamber exudates (white arrow); (b) Occlusion of pupil (white arrow); (c) Posterior synechia with exudate in the pupil area; (d) Whitish appearance of the inferior iris (white arrow); (e, f) Iris nodules (white arrows); (g) OCT view of “net”-like anterior chamber exudates (white arrow); (h) Exudative membrane around the pupil on OCT (white arrow); (i, j) Residual anterior chamber exudates exhibited sporadic patches (white arrow) or fine dots with high reflectivity on OCT. Original magnification of slit-lamp images, × 25 magnification; AS-OCT, anterior segment optical coherence tomography; dpi, days postinfection.

TABLE 1. Clinical Manifestations of CMV Keratouveitis in the Rats of MCMV Group

No. of Rats	Corneal and Conjunctival Signs					Iris Signs				
	Giliary Injection	Localized Corneal Edema	Diffuse Corneal Edema	Mutton Fat Kps	Neovascularization	Iris Hyperemia	Anterior Chamber Exudation	Posterior Synechia	Occlusion of Pupil	Iris Nodules
1	+	-	+	+	+	+	+	+	-	-
2	+	+	-	+	-	+	+	+	+	+
3	+	+	+	+	+	+	+	+	+	-
4	+	+	+	-	-	+	+	+	+	-
5	+	+	-	+	-	+	+	+	+	-
6	+	-	-	+	-	+	+	+	-	+
7	+	+	-	+	-	+	+	+	-	+
8	+	-	+	+	+	+	+	-	-	-
Incidence of different clinical signs										
<i>n</i> (<i>N</i>)	8 (8)	5 (8)	4 (8)	7 (8)	3 (8)	8 (8)	8 (8)	7 (8)	4 (8)	3 (8)
	100%	62.5%	50%	87.5%	37.5%	100%	100%	87.5%	50%	37.5%

n = number of rats with different clinical signs; *N* = 8; + represented the occurrence of corresponding clinical signs on one or more dpi (day postinfection) during the whole period after infection.

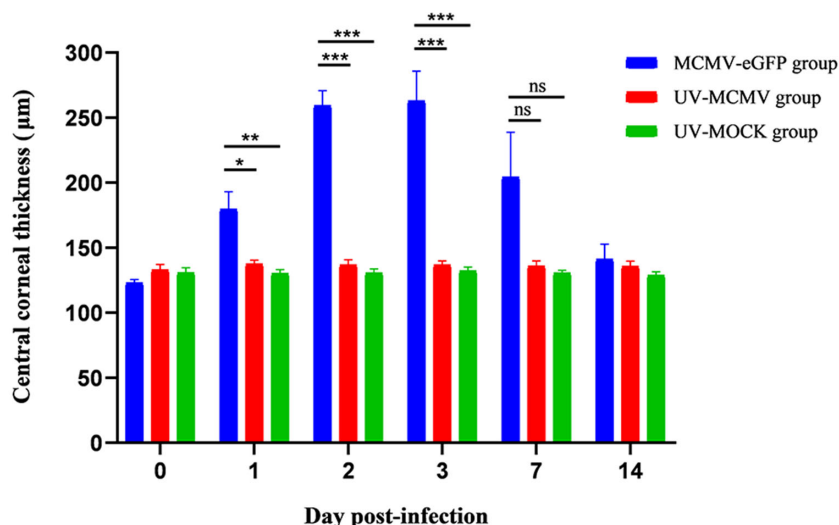


FIGURE 3. Changes in the CCT in the rats of different groups by AS-OCT. *N* = 8 rats in every group; Short bar (comparison of the CCT between the MCMV-eGFP group and the UV-MCMV group by *t*-test); Long bar (comparison of the CCT between the MCMV-eGFP group and the UV-MOCK group by *t*-test); **P* < 0.05; ***P* < 0.01; ****P* < 0.001; CCT, central corneal thickness; AS-OCT, anterior segment optical coherence tomography.

TABLE 2. Incidence of Different Corneal Lesions at Different Time Points by IVCM Among the Rats of MCMV Group

Types of Corneal Lesions by IVCM	Day Postinfection						<i>P</i> Value*
	<i>n</i> / <i>N</i> (%)						
	0	1	2	3	7	14	
“Black holes”	0/8 (0%)	4/8 (50%)	2/8 (25%)	3/8 (37.5%)	2/8 (25%)	2/8 (25%)	0.386
Enlarged intercellular gaps	0/8 (0%)	3/8 (37.5%)	4/8 (50%)	3/8 (37.5%)	2/8 (25%)	2/8 (25%)	0.370
Inflammatory cell infiltration	0/8 (0%)	1/8 (12.5%)	2/8 (25%)	4/8 (50%)	6/8 (75%)	2/8 (25%)	0.019
Hyper-reflective Kps	0/8 (0%)	7/8 (87.5%)	7/8 (87.5%)	5/8 (62.5%)	7/8 (87.5%)	3/8 (37.5%)	<0.001
Bright nuclear cells	0/8 (0%)	1/8 (12.5%)	3/8 (37.5%)	3/8 (37.5%)	4/8 (50%)	2/8 (25%)	0.274
Blurred endothelial layer	0/8 (0%)	2/8 (25%)	3/8 (37.5%)	3/8 (37.5%)	1/8 (12.5%)	0/8 (0%)	0.180

n = number of rats with different types of endothelial changes at different time points; *N* = 8, total number; *P* value* was the results of comparing number of rats with different endothelial changes at different dpi by Fisher’s exact test; IVCM, in-vivo confocal microscopy.

group ($132.2 \pm 3.0 \mu\text{m}$). Although the mean CCT of the MCMV-eGFP group at 7 dpi was still larger than that of the other two groups, there was no significant difference (*P* = 0.076 compared with that of the UV-MCMV group; *P* = 0.058 compared with that of the UV-MOCK group). The CCT of the MCMV-eGFP group returned to $141.1 \pm 11.6 \mu\text{m}$ after 2 weeks, consistent with the corneal edema recovered based on AS-OCT (see Fig. 2B j).

Acute anterior chamber reactions and iridocyclitis occurred after infection as shown in Figure 2C. Inflammatory exudates that formed as net structures spread over the whole space of the anterior chamber (see Fig. 2C a,g); 87.5% of the rats had posterior synechia (see Fig. 2C c), and 50% exhibited occlusion of the pupil, which is typical of anterior uveitis (see Fig. 2C b). As anterior chamber inflammation resolved, there were remarkable changes in the iris, including heterochromic iris, with a whitish appearance in the inferior part compared with the relatively normal color in the superior part (see Fig. 2C d) and iris nodules resembling Koeppe nodules in Fuch’s syndrome (see Fig. 2C e,f). AS-OCT clearly showed that anterior chamber exudates increased in the early period and gradually disappeared at 7 to 14 dpi (see Fig. 2C g-j).

Viral Infection and Immune Injury Were Both Involved in Corneal Endothelial Inflammation

We evaluated the pathological changes in the corneal endothelium at different levels with IVCM, light microscopy, and electron microscopy. Endothelial involvement based on IVCM is displayed in Figure 4A. Normal RCECs had a regular hexagonal shape. The cytoplasm showed a high reflection area with a black nucleus, whereas the cell borders showed low reflection signals (see Fig. 4A a,b). The endothelial lesions based on IVCM varied with the different intervals as shown in Table 2. In the early period after infection, we noticed endothelial changes, including “black holes” (see Fig. 4A c,d) and enlarged intercellular gaps (see Fig. 4A e). Remarkably, an endothelial cell with a “high reflection” nucleus surrounded by a “dark halo” was noted at 3 dpi (see Fig. 4A f), resembling the “Owl’s Eye cell” in human CMV corneal endotheliitis.²² However, severe corneal edema at 1 to 3 dpi resulted in blurred IVCM images of the endothelial layer in 25 to 37.5% of the rats. With corneal edema gradually alleviated, inflammatory cells infiltrated the endothelial layers (see Fig. 4A g,h), and merged bright nuclei (see Fig. 4A i,j) occurred more frequently. In addition, the

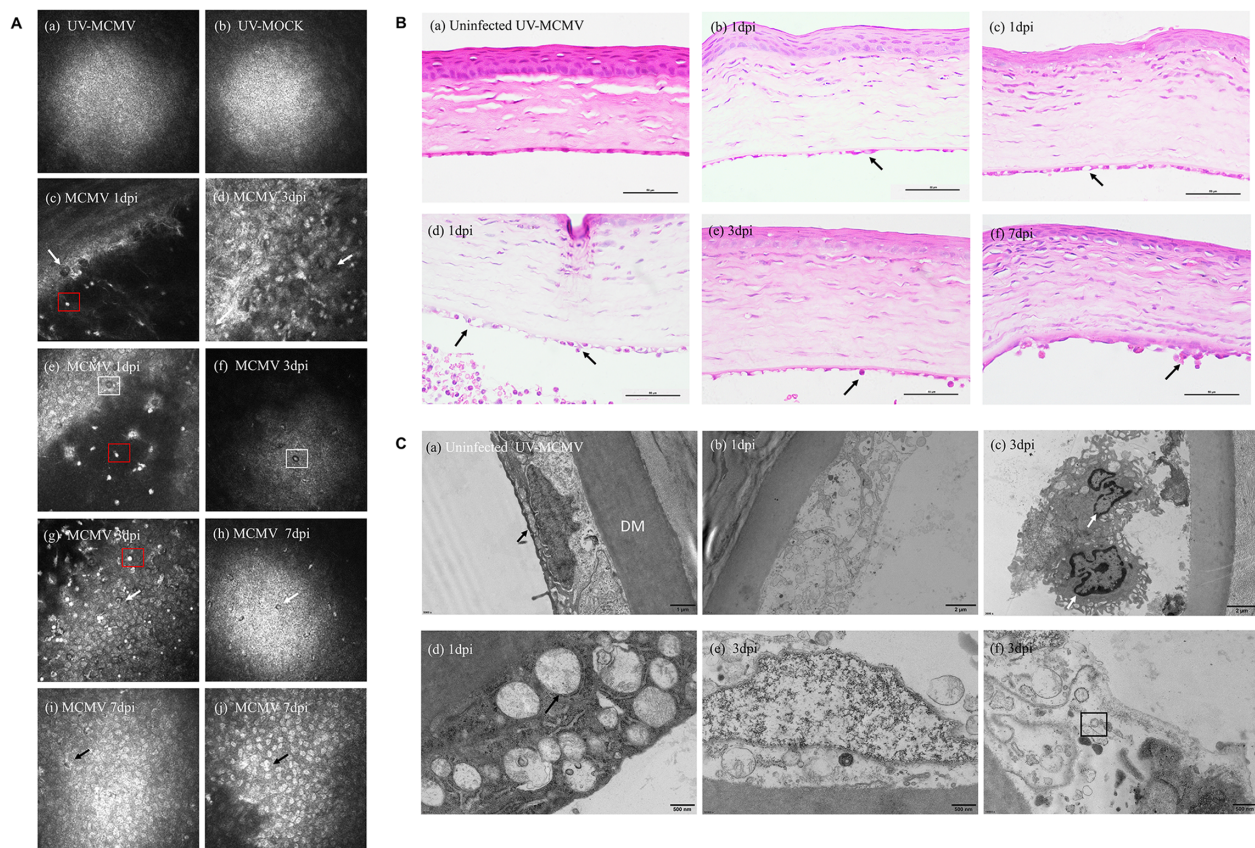


FIGURE 4. Imaging and histopathological changes in the corneal endothelium after infection. (A) IVCM image of the corneal lesions: (a, b) Normal corneal endothelium; (c, d) “Black hole” changes (white arrows); (e) Enlarged intercellular gaps (white square); (f) Distinctive endothelial cell with “high reflection” nucleus surrounded by a dark ring area (white square); (g, h) Inflammatory cellular infiltration (white arrows); (I, j) Endothelial cells with bright nucleus or merged nuclei (black arrows). (B) Representative results of endothelial damage by H&E staining: (a) Normal corneal structure; (b) Swelling of corneal endothelial cells (black arrow); (c) Ballooning degeneration (black arrow); (d) Cell rupture with inflammatory cell infiltration (black arrows); (e, f) Neutrophils and monocytes attached to the injured endothelium (black arrows). Bar = 50 μ m. (C) TEM view of the endothelial layers: (a) Normal endothelial cells full of mitochondria (black arrow); (b) Cell disruption; (c) Endothelium destroyed and infiltrated by monocytes (white arrows); (d) Severe swelling of mitochondria (black arrow); (e) Nuclear edema with mitochondrial damage; (f) Viral envelope within the cytoplasm (black square). IVCM, in vivo confocal microscopy; TEM, transmission electron microscopy; dpi, days postinfection.

hyper-reflective dots that represented inflammatory KPs (see Fig. 4A red squares) adherent to the endothelium lasted for the whole infectious period. Among all the IVCM changes, inflammatory cell infiltration, and KPs showed significant differences, with $P = 0.019$ and $P < 0.001$, respectively.

In accordance with the endothelial changes observed with IVCM, we discovered the corresponding histological lesions with H&E staining. The normal endothelial layer was flat with monolayer cells (Fig. 4B a). After infection, the endothelial layer became uneven with cellular swelling (see Fig. 4B b) and “ballooning degeneration” (see Fig. 4B c); large numbers of neutrophils and monocytes intruded into the endothelial cells, leading to cell rupture (see Fig. 4B d), which was observed in IVCM images as shown in Figure 4A g, h. In addition, an inflammatory cell mass attached to the endothelium (see Fig. 4B f) was observed as KPs and highly reflective round dots in IVCM images.

TEM showed the detailed cytopathic changes in corneal endothelial cells. Corneas with UV-MCMV inoculation showed the normal morphological features of RCECs, in which abundant mitochondria provided adequate energy for maintaining Na^+/K^+ -ATPase pump function (Fig. 4C a). However, corneas with MCMV infection showed obvious

cytotoxic changes in the endothelium. In the early postinfection period, cell disruption (see Fig. 4C b), cell nucleus swelling (see Fig. 4C e) and infiltration of monocytes into the defective area of the endothelium (see Fig. 4C c) were noted. In addition, severe mitochondrial swelling with fracture or loss of crista structure was the most predominant organelle lesion (see Fig. 4C d). A typical viral envelope with a bilayer was also found in the cytoplasm of the destroyed endothelial cells (see Fig. 4C f).

CMV Infection Caused Pathological Changes in the Anterior Chamber Angle, Thus Leading to Elevated IOP

We used an iCare tonometer to monitor the IOP changes in the rats at different time points after infection. As Figure 5A shows, the mean IOP values of the dexamethasone-treated eyes and untreated contralateral eyes were 12.95 ± 0.47 mm Hg (mean \pm SEM) and 12.90 ± 0.43 mm Hg, respectively, with no significant difference ($P = 0.92$). In the UV-MCMV group and UV-MOCK group, the rat IOP values remained in the normal range without significant changes.

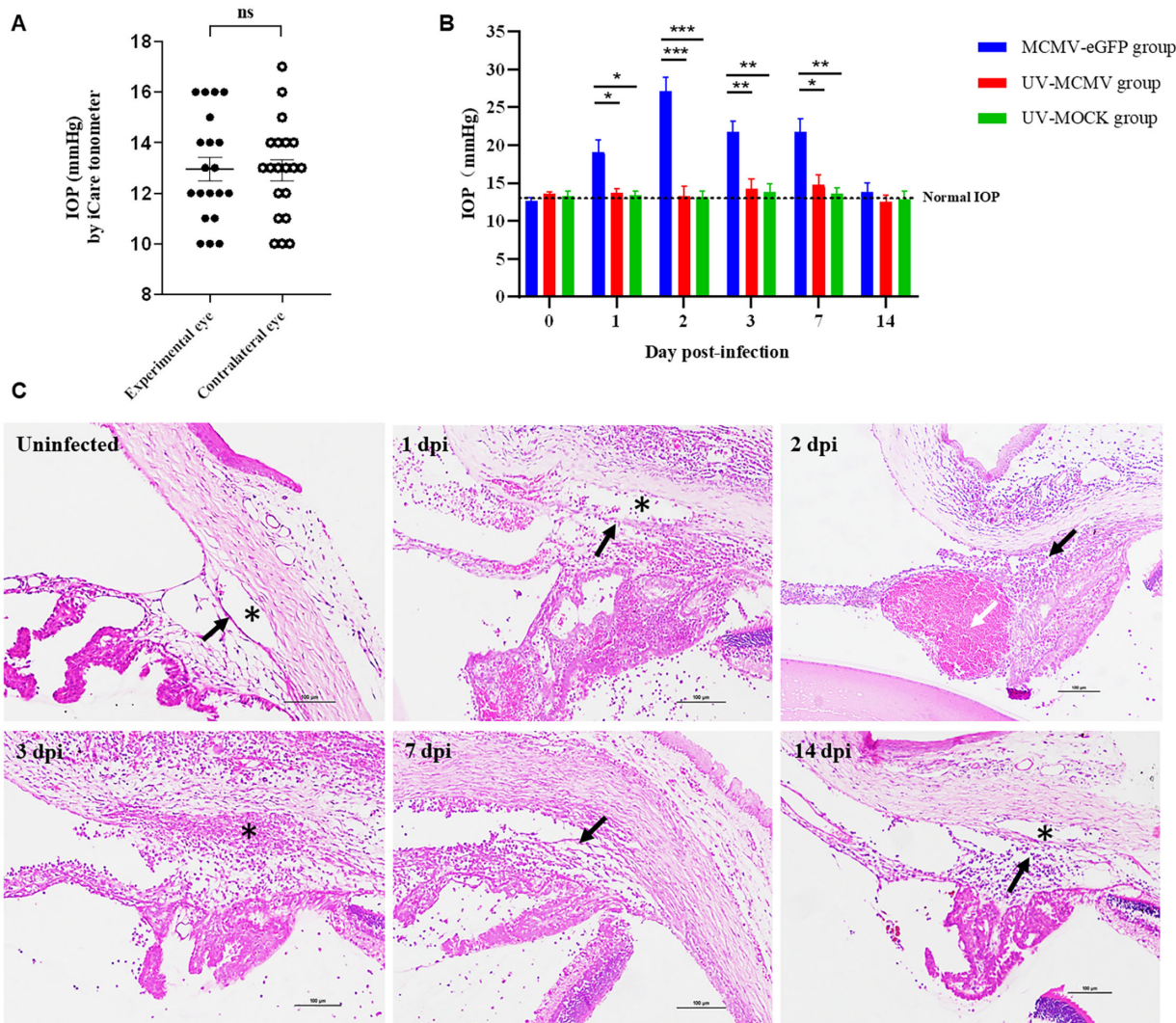


FIGURE 5. IOP fluctuation and corresponding pathological changes in the anterior chamber segment. (A) The distribution of IOP in dexamethasone-treated experimental eyes and untreated contralateral eyes. (Based on the IOP values of 20 rats by iCare tonometer.) (B) The fluctuations in the IOP over postinfection time in different groups were graphed as the mean \pm SEM. Short bar (comparison of the IOP between the MCMV-eGFP group and the UV-MCMV group by *t*-test); Long bar (comparison of the IOP between the MCMV-eGFP group and the UV-MOCK group by *t*-test). **P* < 0.05; ***P* < 0.01; ****P* < 0.001. (C) Inflammation of the structure of the anterior chamber angle by H&E staining: TM structure (black arrows); Schlemm’s canal (* labeled); Hemorrhage in the ciliary body (white arrow). Bar = 100 μ m; IOP, intraocular pressure; dpi, days postinfection.

In sharp contrast, the MCMV group experienced significant IOP elevation in the first week after infection ($P < 0.05$, compared with those in the UV-MCMV and UV-MOCK groups), and the IOP peaked at 27.10 ± 1.84 mm Hg at 2 dpi (Fig. 5B). The IOP values gradually returned to normal after 2 weeks.

Histological analysis revealed obvious inflammatory damage to the TM, Schlemm’s canal, and adjacent tissue (Fig. 5C), which was responsible for the fluctuation in the IOP. Trabeculitis occurred immediately on the first day after MCMV infection and manifested as trabecular endothelial cell swelling and inflammatory cell infiltration (see Fig. 5C, 1 dpi). Due to defects in the blood aqueous barrier, large numbers of inflammatory cells, fibrins, and protein debris accumulated in the anterior chamber angle, directly leading to the mechanical obstruction of the TM and Schlemm’s canal, as shown in Figure 5C (3 dpi). In addition, hemorrhage in the ciliary body was noted at 2 dpi with leakage of red cells confined by fibrous inflammatory tissue (see

Fig. 5C, white arrow). This “hematoma”-like change was responsible for the severe narrowing of the anterior chamber angle, accounting for the peak mean IOP at 2 dpi. In fact, all the above factors together contributed to the elevation of IOP by increasing the aqueous outflow resistance. With the passage of time, the inflammation of the anterior segment gradually resolved after 1 week, and the IOP subsequently declined. We noticed that the IOP values in the MCMV group were still above the upper limit at 7 dpi (see Fig. 5B), and several mutton fat KPs could be spotted with mild anterior chamber reactions (see Fig. 2B f), the combined features of which strikingly resembled PSS.

Inflammation of the Iris and Ciliary Body was Acute and Lasting

Sustained and strong inflammation of the iris and ciliary body was induced by MCMV infection, consistent with the fact that severe iridocyclitis was noted. The iris was

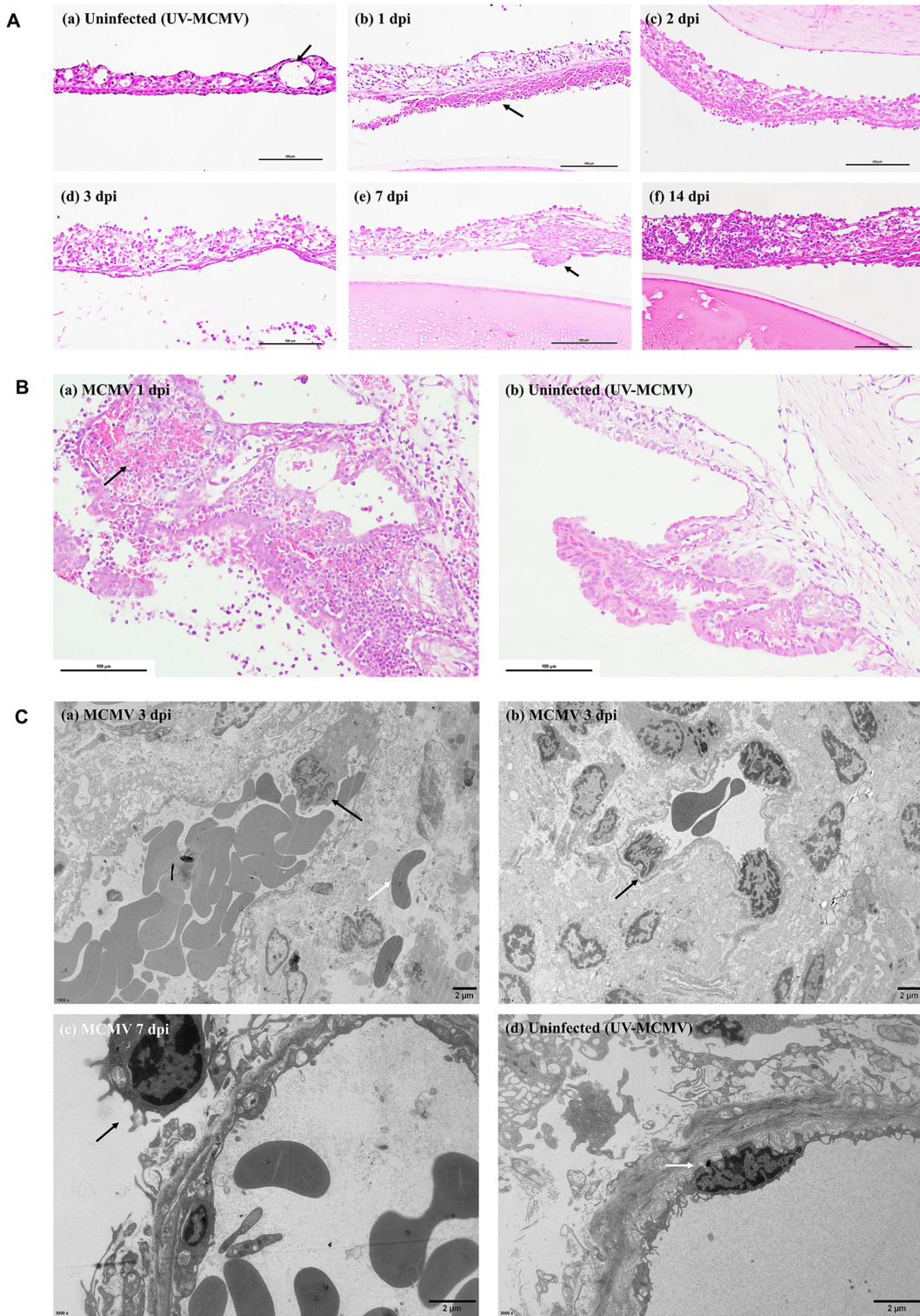


FIGURE 6. Pathological changes in the iris and ciliary body based on light microscopy and TEM. (A) Histological examination of the iris at different postinfection times by H&E staining: (a) Normal blood vessel of the iris (black arrow); (b) Leakage of red cells and exudation of inflammatory cells and fibrins due to the disruption of the blood-aqueous barrier (black arrow); (c, d) Iris edema and infiltration of inflammatory cells; (e) Fibrous membrane on the iris (black arrow); (f) Thickened iris with lymphocyte infiltration on 14 dpi. Bar = 100 μ m. (B) Representative image of ciliary body lesions after MCMV infection: (a) Vascular congestion (black arrow) with large numbers of neutrophils infiltrating into the stroma (white arrow); (b) Normal ciliary body of rats in the UV-MCMV group. Bar = 100 μ m. (C) TEM view of the iris after infection: (a, b) Migrating monocytes that deformed and adhered to the vascular wall (black arrows), red cell leakage through the disrupted vascular wall (white arrow); (c) Monocyte infiltration (black arrow); (d) Normal vascular endothelial cell of the iris.

thickened with cellular edema and inflammatory cell infiltration, lasting for as long as 2 weeks after infection (Fig. 6A). Inflammatory exudates attached to the iris were cellular deposits composed of neutrophils, erythrocytes, and fibrins based on light microscopy observation (see Fig. 6A b). For the ciliary body, there was obvious vascular congestion and large numbers of neutrophils infiltrating the surface and stroma of the ciliary body (Fig. 6B). Electron microscopy showed similar findings: the dilated blood vessel was full of erythrocytes and monocytes, the latter of which attached to the vascular wall, migrating to the damaged tissue and becoming macrophages (Fig. 6C, black arrows).

MCMV Broadly Infected the Anterior Segment Tissue of Rats

To trace the locations of viral infection during the whole process, we infected the rats with recombinant MCMV-eGFP capable of expressing green fluorescence when replicating. Two-photon microscopy was then used to examine the whole cornea buttons and frozen sections of the rat eyes obtained at different time points. The nuclei and F-actin were stained with blue and red signals, respectively, via Hoechst and phalloidin staining.

The infected cells were identified at the endothelium level of the corneal buttons at 1 dpi (Fig. 7A a). The endothelial cells infected with MCMV contained strong green fluorescence in the cytoplasm surrounded by the red-fluorescent cell membrane (see Fig. 7 d,e). Patchy detachment of the endothelial cells from Descemet's membrane was noted at 3 dpi (see Fig. 7A b) and infected endothelial cell swelled with an enlarged black zone in the cytoplasm (see Fig. 7A f). The endothelial cells in the UV-MCMV group showed a hexagonal shape without pathological changes (see Fig. 7A c,g). In addition, in the frozen sections, we found infected endothelial cells with green signals at 1 to 3 dpi (Fig. 7B) and some interacted with inflammatory cells (see Fig. 7B a).

We detected many infected iris cells at 3 dpi (Fig. 7C a-c), and inflammatory hyperplasia of pupil margins (see Fig. 7C f) was noted, corresponding with iris nodules observed with slit-lamp examination (see Fig. 7C d). In addition, MCMV infected many monocytes (Fig. 7D) with round shapes and were distinguished from the polygonal endothelial cells. TM cells were also infected with MCMV, with no exception at 1 to 3 dpi (Fig. 7E), which accounted for the trabeculitis and the elevated IOP.

Consistent with the results of the two-photon microscopy examination, MCMV IE RNA was detected in the anterior segment tissue of the MCMV-eGFP group at 1 to 3 dpi (Fig. 8 white square). The results demonstrated that MCMV could infect the anterior segment tissue of rats in the early postinfection period and express viral mRNA, whereas the retina was free from viral infection according to the RT-PCR examination (see Fig. 8).

DISCUSSION

After multiple pilot experiments, we optimized the protocol by topical use of steroids first followed by intracameral inoculation of an appropriate viral titer of MCMV to finally establish an animal model of CMV keratouveitis in rats. CMV keratouveitis was characterized by an acute phase of concomitant corneal endotheliitis and hypertensive anterior uveitis, which lasted for 7 to 14 days. We discovered

that the manifestations of CMV anterior segment infection transformed remarkably into different syndromes resembling certain human diseases over time. In the early phase (1–3 dpi), the experimental rats developed localized or diffuse corneal edema with endothelial damage by imaging tests, supporting the diagnosis of corneal endotheliitis. However, with corneal edema and anterior chamber inflammation relieved, we noted sporadic mutton fat KPs with a raised IOP (3–7 dpi), the features of which were consistent with PSS. At 7 to 14 dpi, the iris color change and iris nodules (see Fig. 2C d–f) were similar to those of Fuch's syndrome to some extent. All the above findings seemed to reveal that these syndromes might share the common etiological factor of CMV infection. In real clinical practice, Oka et al.²³ discovered that patients with CMV endotheliitis or iridocyclitis mostly had the same viral genotype of gB type 1. Previous studies have suggested that CMV is capable of infecting corneal endothelial cells^{24,25} and TM cells^{26,27} in vitro and causes specific cytopathic changes. In addition, Voigt et al.²⁸ demonstrated that MCMV tends to infect the uvea in mice through systemic infection and to induce sustained inflammation. Here, we are the first to report that CMV could infect the corneal endothelium (1–3 dpi), iris (2–3 dpi), TM cells (1–3 dpi), and monocytes (1–3 dpi) in vivo (see Fig. 7) and caused prolonged inflammatory reactions in different compartments of the anterior chamber. In addition, MCMV IE RNA was detected in the anterior segments from 1 to 3 dpi. All the experimental evidence supported the concept that CMV could widely infect ocular anterior segment tissue and induce the corresponding clinical features. Corneal endotheliitis and hypertensive anterior uveitis, including PSS and Fuch's syndrome, are very likely the specific stages of CMV anterior segment infection.

CMV endotheliitis and anterior uveitis usually occur in immunocompetent patients; however, most of these patients have one or more risk factors for local immune suppression, such as being middle-aged or older⁹; having a history of ocular surgery including keratoplasty and cataract surgery^{29–34}; and having a history of use of topical steroids and immunosuppressants.^{9,35} Combined with the mild to moderate anterior chamber inflammation observed in CMV-associated infection, we assumed that topical immunosuppression was an important feature of the ocular microenvironment in these patients. Therefore, we applied topical glucocorticoids before injection of the virus to establish the animal model of CMV keratouveitis. The inflammatory response in the experimental group was partially suppressed, as expected, and there was no evidence of severe hypopyon or tendency to endophthalmitis, which we had seen in the pilot experiment with direct injection of the same amount of MCMV instead. The pathogenesis of CMV anterior segment infection is far from clear. Zheng et al.^{36,37} once established a herpes simplex virus (HSV) corneal endotheliitis model in rabbits to verify the hypothesis of anterior chamber-associated immune deviation. Although both HSV and CMV belong to the Herpesviridae family, they exhibit different routes of ocular infection and methods of reactivation. It is well known that HSV can travel retrograde to the trigeminal ganglia after primary infection and spread via sensory nerves to specific sites of the eye when reactivated.³⁸ Therefore, it is likely that HSV intermittently spreads via the nasociliary nerve to the iris and ciliary body, causing anterior uveitis and further shedding into the anterior chamber, involving the corneal endothelium. In contrast, CMV mainly infects CD34+ myeloid progenitor cells to establish

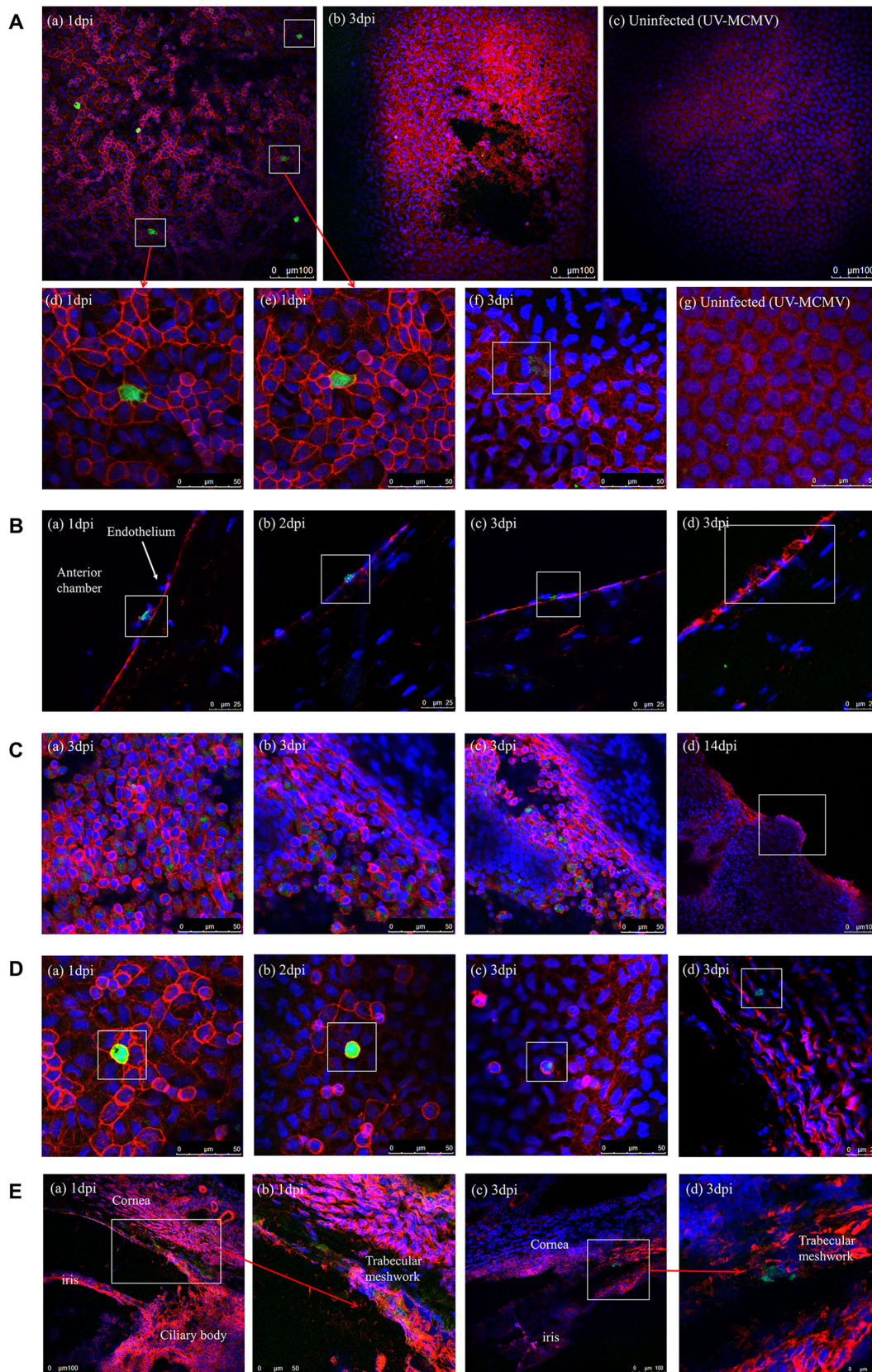


FIGURE 7. MCMV infection site detection by immunofluorescence examination. (A) Infection sites of MCMV in the endothelial layer: (a) Multiple infected endothelial cells expressing green fluorescence at 1 dpi (white squares); (b) Patchy necrosis and detachment of endothelium noted at 3 dpi; (c) Endothelial layer without signs of infection in the UV-MCMV group; (d, e) Enlarged images of infected endothelial cells with white squares in picture-a; (f) Swelled endothelial cells with mild green signals within the cytoplasm (white square); (g) Uninfected normal endothelium. (B) Identification of MCMV infection sites on frozen sections: (a) Infected endothelial cells interacting

with two inflammatory cells identified by blue nuclear markers (white square); (b, c) Infected endothelial cells; (d) Injured endothelial cells with fractured membranes. (C) Infection sites of MCMV in the iris: (a–c) Infected iris cells expressing green fluorescence within the cytoplasm; (d) Hyperplasia of the margin of the pupil representing the iris nodule. (D) Infected monocytes. (E) Infected TM cells in the frozen sections.

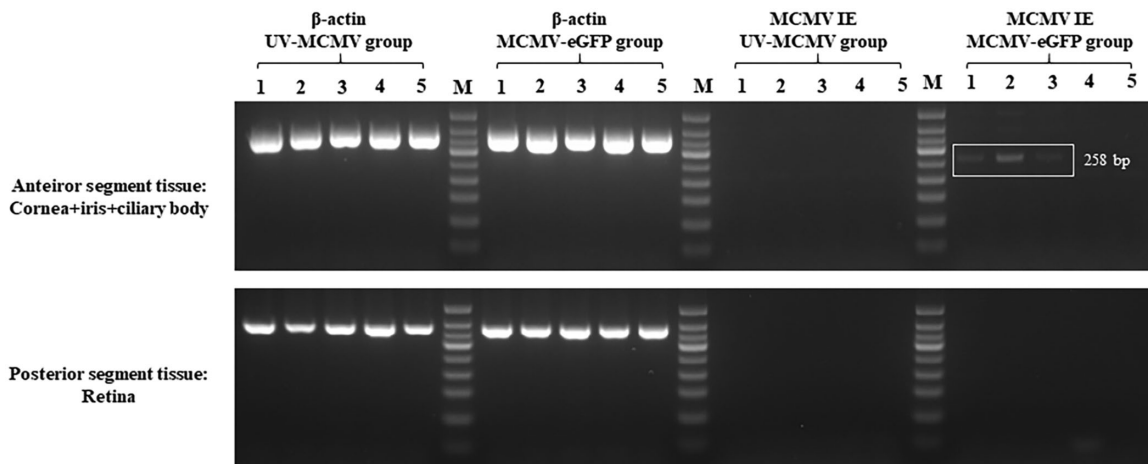


FIGURE 8. Detection of MCMV IE RNA by RT-PCR. All the eyeballs of the rats were divided into two parts: anterior segment tissue, including the dissected cornea, iris and ciliary body, and posterior segment tissue, including the retina. At each time point, samples from four independent rats in each group were pooled for RT-PCR examination. The results are representative of three separate experiments. Lane M, DNA marker; Lanes 1–3, 1–3 dpi; Lane 4, 7 dpi; Lane 5, 14 dpi; dpi, days postinfection.

lifelong latent infection in the bone marrow.³⁹ The latently infected cells could subsequently divide and differentiate into monocytes that mobilize throughout the body via blood circulation. Under the stimulus of specific inflammation, these monocytes could become highly activated and further differentiate into macrophages and dendritic cells, which are capable of shedding CMV viral particles into tissue including the eye.^{39,40} In our study, we found that monocyte-macrophages with MCMV-eGFP (see Fig. 7D) were not rare and often interacted with injured endothelial cells (see Fig. 4C c and Fig. 7B a). Based on these findings, we considered that CMV-infected monocytes might be responsible for anterior segment infection. These monocytes entered the anterior chamber through a disrupted blood aqueous barrier and experienced reactivation with low local immunity, subsequently infecting the corneal endothelium and iris. Further studies are required to test this hypothesis.

In our study, we discovered that the fluctuation in IOP was highly correlated with the severity of pathological changes in the anterior chamber angle structures as shown in Figure 5. Multiple factors combined to contribute to the increased IOP in terms of histopathology. First, we demonstrated that MCMV could infect TM cells in vivo (see Fig. 7E), causing direct inflammation of the TM, also termed trabeculitis. Trabeculitis was characterized by swelling of trabecular lamellae and reduced intertrabecular spaces (see Fig. 5C), which finally increased outflow resistance.⁴¹ In fact, evidence of viral infection of the TM is not rare. Amano et al.⁴² identified HSV in the excised trabecular tissue of a patient with corneal endotheliitis and increased IOP by immunochemical examination. Recently, Singh et al.⁴³ injected Zika virus into the mouse anterior chamber and caused infectivity in the iridocorneal angle and TM, leading to the death of TM cells in the mouse eyes. Similarly,

our study was the first to report that in vivo infection of the TM also occurs in CMV infections. In addition to trabeculitis, mechanical obstruction of the aqueous outflow pathway was another important reason for increased outflow resistance. Due to the disrupted blood-aqueous barrier, large numbers of inflammatory cells and large amounts of fibrins and protein debris precipitated in the anterior chamber angle, blocking the TM and Schlemm's canal (see Fig. 5C). The above theory⁴⁴ is widely accepted to be the pathogenesis of most open-angle glaucoma secondary to uveitis. Moreover, anterior synechia (see Fig. 2B 1 dpi) and narrowing of the anterior chamber angle caused by ciliary body hemorrhage (see Fig. 5C 2 dpi) were also considered to increase IOP. Regardless of whether trabeculitis or inflammatory obstruction of the outflow pathway was the acute reaction of viral infection, both responded well to glucocorticoid treatment. However, single use of anti-inflammatory drugs inhibited the clearing of virus, in turn, which could lead to recurrence in the long run. Therefore, antiviral treatment was also necessary to remove the underlying cause.

Corneal edema was one of the most prominent features in the rats infected with MCMV. Nearly all the rats in the MCMV group developed different degrees of corneal edema from a diffuse pattern to a localized pattern (see Fig. 2B). Even though an increased IOP could cause corneal edema, a localized pattern was more likely to result from endotheliitis, which was confirmed by imaging and pathological tests. IVCN has the advantage of scanning different levels of corneal tissue and showing endothelial lesions, even through the thickened corneas. In IVCN images, the alterations in the endothelium consisted of “black holes,” enlarged intercellular gaps and inflammatory infiltration (see Fig. 4A), all of which have been reported in human HSV endotheliitis.⁴⁵ Therefore, these alterations were not

specific for a certain virus but are common features of viral endotheliitis. Interestingly, we also discovered a distinctive endothelial cell pattern (see Fig. 3A f) similar to “Owl’s eye morphology,” which is believed to indicate CMV endotheliitis.^{22,46–48} Although “Owl’s eye cells” are believed to be specific for CMV endotheliitis compared with CMV diseases in other organs, the sensitivity is relatively low, and nearly half of human cases of CMV endotheliitis⁵ do not exhibit this change. For pathological examination, a series of cytopathic changes were noted, including cell swelling, “balloon degeneration,” and inflammatory cell infiltration into the endothelium (see Fig. 3B c–d), which were highly consistent with the phenomenon observed via IVCM. During the whole infectious process, both viral toxicity and the immune response resulted in the destruction of endothelial cells. This explained why CMV endotheliitis responds well to antiviral treatment and topical steroids^{49,50} in clinical observation. In terms of TEM examination, mitochondrial damage was most remarkable among the organelles of corneal endothelial cells (see Fig. 3C d). Corneal endothelial cells have abundant mitochondria, which provide enough ATP to maintain Na⁺/K⁺-ATPase pump function. This “pump” function and tight junctions between endothelial cells are responsible for maintaining corneal transparency.⁵¹ Previous studies have reported that several endothelial diseases are associated with mitochondrial damage, such as Fuch’s endothelial corneal dystrophy,⁵² diabetes mellitus⁵³ and atropine cytotoxicity to the endothelium.⁵⁴ In this study, MCMV infection combined with acute ocular hypertension⁵¹ compromised normal mitochondrial morphology and function, resulting in corneal edema.

Although the whole course of MCMV infection in rats was an acute phase, inflammation in the iris tended to transform into a chronic form. In the early postinfection period, vascular congestion with cellular infiltration was the most prominent pathological feature of the iris and ciliary body (see Fig. 6); CMV infection of vascular endothelial cells and host immune response to cells expressing viral antigen might be the stimulus for inflammation in the uvea.⁵⁵ In the second week after infection, the replicating virus was no longer detectable in the anterior segment tissue; however, there was still cellular infiltration in the iris (see Fig. 5A f), and iris nodules were noted around the pupillary margins in 37.5% of the rats in the MCMV group (see Fig. 2C e,f). The essence of iris nodules was iris tissue hyperplasia under chronic inflammatory stimulation (see Fig. 7C d), which is prevalent in human Fuch’s syndrome.⁵⁶ Therefore, acute infection of CMV in the anterior segment seemed to induce sustained iris inflammation, which was also supported by the study of Voigt et al.²⁸

Even though mice are the priority for the establishment of animal models of most human diseases, our current study used rats as an alternative to mice for the following reasons. First, we achieved a higher success rate of anterior chamber paracentesis in rats with less damage to adjacent structures. Because we focused mainly on virus-induced anterior segment lesions, it was necessary to ensure no bleeding or injury of the iris, ciliary body, or lens during anterior chamber paracentesis. Due to the tiny space of the mouse anterior chamber, we often injured the iris or ciliary body and caused bleeding after injecting MCMV, which affected the subsequent experiments. Second, rat corneas are more suitable for confocal scanning in vivo and in vitro than mouse corneas. The radius of curvature of mouse corneas is much smaller than that of rat corneas. When exam-

ined with IVCM, mouse corneas showed uneven endothelial layers with poor performance. In fact, the original aim of this animal experiment was to investigate the relationships between the clinical manifestations of CMV infection and imaging and histopathological changes. Therefore, it is important to achieve high-quality imaging results and tissue sections. Third, according to our in vitro cell experiment, MCMV could infect RCECs efficiently even at a low MOI (see Fig. 1). Green-fluorescent-positive RCECs in which MCMV was possibly replicated were noted, and surrounding cells were involved afterward. This result laid a foundation for the next rat model experiment.

There are several limitations in our current study. We identified infected cells with green fluorescence in the anterior segment of rats and detected IE RNA expression. The above evidence proved that MCMV could infect the corresponding tissue but did not sufficiently support the productive replication of MCMV in vivo. In addition, this study lacked immunity indicator testing during the establishment of the animal model, which will require further investigation into the immune cells and cytokines involved in the infectious course.

In summary, our study demonstrated that CMV could give rise to broad infection of anterior segment tissue in vivo, including the corneal endothelium, the iris, the TM, and monocytes. Corneal endotheliitis and HAU could be the specific stage of anterior segment infection of CMV. In addition, both viral infection and the immune response play an important role in the pathogenesis of corneal endothelium and iris injury and elevated IOP. The local immunosuppressive state might be more consistent with the microenvironment of CMV-associated diseases.

Acknowledgments

The authors thank Li Ying for her help with the animal experiments and her guidance regarding the histopathological examinations.

This work was supported by the National Natural Science Foundation of China (81970768 and 81800801) and the Open Research Fund Program of the State Key Laboratory of Virology of China (2020IOV002).

Disclosure: **S. Zhang**, None; **Y. Zang**, None; **Q. Lu**, None; **J. Ma**, None; **X. Jiang**, None; **J. Qu**, None; **J. Zhang**, None; **R. Peng**, None; **M. Luo**, None; **J. Hong**, None

References

1. Koizumi N, Suzuki T, Uno T, et al. Cytomegalovirus as an etiologic factor in corneal endotheliitis. *Ophthalmology*. 2008;115(2):292–297.e293.
2. Chee SP, Jap A. Presumed fuchs heterochromic iridocyclitis and Posner-Schlossman syndrome: comparison of cytomegalovirus-positive and negative eyes. *Am J Ophthalmol*. 2008;146(6):883–889.e881.
3. van Boxtel LA, van der Lelij A, van der Meer J, Los LI. Cytomegalovirus as a cause of anterior uveitis in immunocompetent patients. *Ophthalmology*. 2007;114(7):1358–1362.
4. Koizumi N, Yamasaki K, Kawasaki S, et al. Cytomegalovirus in aqueous humor from an eye with corneal endotheliitis. *Am J Ophthalmol*. 2006;141(3):564–565.
5. Peng RM, Guo YX, Xiao GG, Li CD, Hong J. Characteristics of Corneal Endotheliitis among Different Viruses

- by in Vivo Confocal Microscopy. *Ocul Immunol Inflamm.* 2021;29(2):324–332.
6. Yu T, Peng RM, Xiao GG, Feng LN, Hong J. Clinical Evaluation of Intravitreal Injection of Ganciclovir in Refractory Corneal Endotheliitis. *Ocul Immunol Inflamm.* 2020;28(2):270–280.
 7. Qu JH, Peng RM, Xiao GG, et al. The incidence and influence of the donor corneas positive for herpesviridae DNA in keratoplasty. *Graefes Arch Clin Exp Ophthalmol.* 2020;258(12):2767–2774.
 8. Hsiao CH, Hwang YS, Chuang WY, et al. Prevalence and clinical consequences of cytomegalovirus DNA in the aqueous humour and corneal transplants [published online ahead of print June 28, 2018]. *Br J Ophthalmol*, <https://doi.org/10.1136/bjophthalmol-2018-312196>.
 9. Koizumi N, Inatomi T, Suzuki T, et al. Clinical features and management of cytomegalovirus corneal endotheliitis: analysis of 106 cases from the Japan corneal endotheliitis study. *Br J Ophthalmol.* 2015;99(1):54–58.
 10. Chan NS, Chee SP, Caspers L, Bodaghi B. Clinical Features of CMV-Associated Anterior Uveitis. *Ocul Immunol Inflamm.* 2018;26(1):107–115.
 11. Choi JA, Kim KS, Jung Y, Park HY, Park CK. Cytomegalovirus as a cause of hypertensive anterior uveitis in immunocompetent patients. *J Ophthalmic Inflamm Infect.* 2016;6(1):32.
 12. Chee SP, Jap A. Cytomegalovirus anterior uveitis: outcome of treatment. *Br J Ophthalmol.* 2010;94(12):1648–1652.
 13. Chee SP, Bacsal K, Jap A, Se-Thoe SY, Cheng CL, Tan BH. Clinical features of cytomegalovirus anterior uveitis in immunocompetent patients. *Am J Ophthalmol.* 2008;145(5):834–840.
 14. Khieu C, Kongyai N, Pathanapitoon K, Van Der Eijk AA, Rothova A. Causes of Hypertensive Anterior Uveitis in Thailand. *Ocul Immunol Inflamm.* 2020;28(4):559–565.
 15. Touhami S, Qu L, Angi M, et al. Cytomegalovirus Anterior Uveitis: Clinical Characteristics and Long-term Outcomes in a French Series. *Am J Ophthalmol.* 2018;194:134–142.
 16. Antoun J, Willermain F, Makhoul D, Motulsky E, Caspers L, Relvas LJ. Topical Ganciclovir in Cytomegalovirus Anterior Uveitis. *J Ocul Pharmacol Ther.* 2017;33(4):313–318.
 17. Accorinti M, Gilardi M, Pirraglia MP, et al. Cytomegalovirus anterior uveitis: long-term follow-up of immunocompetent patients. *Graefes Arch Clin Exp Ophthalmol.* 2014;252(11):1817–1824.
 18. Kam KW, Leung KS, Kwok RPW, et al. Clinical features, diagnosis and treatment outcomes of cytomegalovirus endotheliitis in Hong Kong. *Acta Ophthalmol.* 2018;96(4):e541–e542.
 19. Miyayama M, Sugita S, Shimizu N, et al. A significant association of viral loads with corneal endothelial cell damage in cytomegalovirus anterior uveitis. *Br J Ophthalmol.* 2010;94(3):336–340.
 20. Lu Q, Sun BJ, Zhou YP, et al. Pathogenic Effects and Pathogenesis Processes in Vitro & in Vivo in Murine Cytomegalovirus Infected Rat Corneal Endothelial Cells [published online ahead of print November 23, 2020]. *Ocul Immunol Inflamm*, <https://doi.org/10.1080/09273948.2020.1833941>.
 21. Yuhasz SA, Dissette VB, Cook ML, Stevens JG. Murine cytomegalovirus is present in both chronic active and latent states in persistently infected mice. *Virology.* 1994;202(1):272–280.
 22. Shiraishi A, Hara Y, Takahashi M, et al. Demonstration of “owl’s eye” morphology by confocal microscopy in a patient with presumed cytomegalovirus corneal endotheliitis. *Am J Ophthalmol.* 2007;143(4):715–717.
 23. Oka N, Suzuki T, Inoue T, Kobayashi T, Ohashi Y. Polymorphisms in cytomegalovirus genotype in immunocompetent patients with corneal endotheliitis or iridocyclitis. *J Med Virol.* 2015;87(8):1441–1445.
 24. Miyazaki D, Uotani R, Inoue M, et al. Corneal endothelial cells activate innate and acquired arm of anti-viral responses after cytomegalovirus infection. *Exp Eye Res.* 2017;161:143–152.
 25. Hosogai M, Shima N, Nakatani Y, et al. Analysis of human cytomegalovirus replication in primary cultured human corneal endothelial cells. *Br J Ophthalmol.* 2015;99(11):1583–1590.
 26. Shimizu D, Miyazaki D, Shimizu Y, Hosogai M, Kosugi I, Inoue Y. Infection of endotheliotropic human cytomegalovirus of trabecular meshwork cells. *Jpn J Ophthalmol.* 2018;62(6):667–676.
 27. Choi JA, Kim JE, Noh SJ, Kyoung Kim E, Park CK, Paik SY. Enhanced cytomegalovirus infection in human trabecular meshwork cells and its implication in glaucoma pathogenesis. *Sci Rep.* 2017;7(1):43349.
 28. Voigt V, Andoniou CE, Schuster IS, et al. Cytomegalovirus establishes a latent reservoir and triggers long-lasting inflammation in the eye. *PLoS Pathog.* 2018;14(5):e1007040.
 29. Tan TE, Tan DTH. Cytomegalovirus Corneal Endotheliitis After Descemet Membrane Endothelial Keratoplasty. *Cornea.* 2019;38(4):413–418.
 30. Wang H, Zheng J, Zheng Q, et al. Incidence and Risk Factors of New Onset Endotheliitis After Cataract Surgery. *Invest Ophthalmol Vis Sci.* 2018;59(12):5210–5216.
 31. Tan TE, Cheung CM, Mehta JS. Activation of Cytomegalovirus corneal endotheliitis following laser in situ keratomileusis. *BMJ Case Rep.* 2016;2016:bcr2016216774.
 32. Chee SP, Jap A, Ling EC, Ti SE. Cytomegalovirus-positive corneal stromal edema with keratic precipitates after penetrating keratoplasty: a case-control study. *Cornea.* 2013;32(8):1094–1098.
 33. Zamir E, Stawell R, Jhanji V, Vajpayee RB. Corneal endotheliitis triggered by cataract surgery in a Chinese patient with cytomegalovirus anterior uveitis. *Clin Exp Ophthalmol.* 2011;39(9):913–915.
 34. Wang SC, Tsai IL, Lin HC, Kuo LL, Tsai CY, Liou SW. Recurrent cytomegalovirus corneal endotheliitis after penetrating keratoplasty. *Eur J Ophthalmol.* 2010;20(2):457–459.
 35. Siak J, Chee SP. Cytomegalovirus Anterior Uveitis Following Topical Cyclosporine A. *Ocul Immunol Inflamm.* 2018;26(1):90–93.
 36. Zheng X, Ohashi Y. Understanding corneal endotheliitis: an animal model approach. *Int Ophthalmol Clin.* 2002;42(1):151–156.
 37. Zheng X, Yamaguchi M, Goto T, Okamoto S, Ohashi Y. Experimental corneal endotheliitis in rabbit. *Invest Ophthalmol Vis Sci.* 2000;41(2):377–385.
 38. Farooq AV, Shukla D. Corneal latency and transmission of herpes simplex virus-1. *Fut Virol.* 2011;6(1):101–108.
 39. Sinclair J, Reeves M. The intimate relationship between human cytomegalovirus and the dendritic cell lineage. *Front Microbiol.* 2014;5:389.
 40. Carmichael A. Cytomegalovirus and the eye. *Eye (Lond).* 2012;26(2):237–240.
 41. Sng CC, Ang M, Barton K. Uveitis and glaucoma: new insights in the pathogenesis and treatment. *Prog Brain Res.* 2015;221:243–269.
 42. Amano S, Oshika T, Kaji Y, Numaga J, Matsubara M, Araie M. Herpes simplex virus in the trabeculum of an eye with corneal endotheliitis. *Am J Ophthalmol.* 1999;127(6):721–722.

43. Singh PK, Kasetti RB, Zode GS, Goyal A, Juzych MS, Kumar A. Zika Virus Infects Trabecular Meshwork and Causes Trabeculitis and Glaucomatous Pathology in Mouse Eyes. *mSphere*. 2019;4(3):e00173–e00219.
44. Siddique SS, Suelves AM, Baheti U, Foster CS. Glaucoma and uveitis. *Surv Ophthalmol*. 2013;58(1):1–10.
45. Hillenaar T, Weenen C, Wubbels RJ, Remeijer L. Endothelial involvement in herpes simplex virus keratitis: an in vivo confocal microscopy study. *Ophthalmology*. 2009;116(11):2077–2086.e2071-e2072.
46. Yokogawa H, Kobayashi A, Yamazaki N, Sugiyama K. In vivo imaging of coin-shaped lesions in cytomegalovirus corneal endotheliitis by anterior segment optical coherence tomography. *Cornea*. 2014;33(12):1332–1335.
47. Yokogawa H, Kobayashi A, Sugiyama K. Mapping owl's eye cells of patients with cytomegalovirus corneal endotheliitis using in vivo laser confocal microscopy. *Jpn J Ophthalmol*. 2013;57(1):80–84.
48. Kobayashi A, Yokogawa H, Higashide T, Nitta K, Sugiyama K. Clinical significance of owl eye morphologic features by in vivo laser confocal microscopy in patients with cytomegalovirus corneal endotheliitis. *Am J Ophthalmol*. 2012;153(3):445–453.
49. Hwang JH, Ha M, Park Y, Chung SH. The Effect of Topical Ganciclovir and Corticosteroid on Cytomegalovirus Corneal Endotheliitis in Korean Patients. *Ocul Immunol Inflamm*. 2019;27:338–344.
50. Fan NW, Chung YC, Liu YC, Liu CJ, Kuo YS, Lin PY. Long-Term Topical Ganciclovir and Corticosteroids Preserve Corneal Endothelial Function in Cytomegalovirus Corneal Endotheliitis. *Cornea*. 2016;35(5):596–601.
51. Li X, Zhang Z, Ye L, et al. Acute ocular hypertension disrupts barrier integrity and pump function in rat corneal endothelial cells. *Sci Rep*. 2017;7(1):6951.
52. Miyai T. Fuchs Endothelial Corneal Dystrophy and Mitochondria. *Cornea*. 2018;37(Suppl 1):S74–S77.
53. Aldrich BT, Schlotzer-Schrehardt U, Skeie JM, et al. Mitochondrial and Morphologic Alterations in Native Human Corneal Endothelial Cells Associated With Diabetes Mellitus. *Invest Ophthalmol Vis Sci*. 2017;58(4):2130–2138.
54. Wen Q, Fan TJ, Tian CL. Cytotoxicity of atropine to human corneal endothelial cells by inducing mitochondrion-dependent apoptosis. *Exp Biol Med (Maywood)*. 2016;241(13):1457–1465.
55. Golden MP, Hammer SM, Wanke CA, Albrecht MA. Cytomegalovirus vasculitis. Case reports and review of the literature. *Medicine (Baltimore)*. 1994;73(5):246–255.
56. Sun Y, Ji Y. A literature review on Fuchs uveitis syndrome: An update. *Surv Ophthalmol*. 2020;65(2):133–143.